A short-duration pulse of ductile normal shear on the outer South Tibetan detachment in Bhutan: Alternating channel flow and critical taper mechanics of the eastern Himalaya

Jennifer Chambers,[1] Randall Parrish,[2,3] Tom Argles,[4] Nigel Harris,[4] and Matthew Horstwood[3]

Received 31 August 2010; revised 21 December 2010; accepted 4 January 2011; published 11 March 2011.

[1] In easternmost Bhutan the South Tibetan detachment (STD) is a ductile shear zone that juxtaposes the Radi (or Sakteng) klippe of the Tethyan Sedimentary Series from underlying high-grade Greater Himalayan rocks. In situ LA-ICPMS U-Th-Pb analysis of metamorphic monazite from the immediate footwall and hanging wall of the STD within the shear zone at the base of the klippe, constrains north vergent normal shear to between 25 and 20 Ma. Coeval thrusting on the Main Central Thrust during this time supports a phase of channel flow–viscous wedge model activity, lasting only ~3 Ma. Geochronologic data from the eastern Himalaya indicate alternating mechanisms for extrusion of the metamorphic core of the orogen from the Late Oligocene through to the Late Miocene, switching from channel flow–viscous wedge behavior to critical taper–frictional wedge behavior, each phase lasting approximately only 2 to 5 Ma. The tectonic evolution of the eastern Himalaya is comparable to central and western Himalayan tectonics during the Early Miocene, but during the Middle Miocene metamorphism and magmatism in the eastern Himalaya migrated toward the orogenic hinterland, a process not widely documented elsewhere in the Himalaya, thus highlighting the need for an orogenic model in three spatial dimensions. **Citation:** Chambers, J., R. Parrish, T. Argles, N. Harris, and M. Horstwood (2011), A short-duration pulse of ductile normal shear on the outer South Tibetan detachment in Bhutan: Alternating channel flow and critical taper mechanics of the eastern Himalaya, *Tectonics*, *30*, TC2005, doi:10.1029/2010TC002784.

1. Introduction

[2] The Himalayan orogen, formed in response to the collision between India and Eurasia by ~50 Ma (see review in the work of *Najman et al.* [2010]), represents the archetypal modern continent-continent collision zone. The metamorphic core, the Greater Himalayan Sequence (GHS), is bound by the Main Central Thrust [e.g., *Heim and Gansser*, 1939] below and the South Tibetan Detachment (STD) [*Burchfiel et al.*, 1992] above. These major crustal-scale fault systems can be traced near continuously along the 2200 km length of the orogen, yet we do not fully understand the evolution of these structures in time and/or space, compromising tectonic models for the Himalaya and for modern orogenesis in general. For example, the evidence for sustained coeval thrusting on the MCT and normal shear on the STD throughout the Early Miocene (23–16 Ma) [*Godin et al.*, 2006, Table 1] supports models of wedge or channel-like extrusion of the GHS [e.g., *Jamieson et al.*, 2004]. *Leloup et al.* [2010] establish that the switch from movement on the STD in southern Tibet, north of eastern Nepal, to exhumation on north-south trending normal faults at circa 12 Ma is coeval with changes in the basal thrust configuration that is more consistent with wedge extrusion than channel flow, at least by the mid-Miocene. However, the MCT-STD branch line geometry and alternating kinematics recorded on the STD generate contrasting tectonic wedge models, e.g., for the western Himalaya [*Yin*, 2006; *Webb et al.*, 2007]. Alternatively, a critical taper model based on data from Nepal in the central Himalaya [*Kohn*, 2008] suggests that the STD played a relatively minor role in the thermomechanics of the orogenic wedge compared to the MCT. It is therefore evident that the timing, duration and kinematics of slip on these faults forms a critical test of the aforementioned models for Himalayan orogenesis.

[3] The tectonic architecture of the Bhutan Himalaya features discrete inner and outer (relative to the hinterland) strands of the STD (Figure 1 [*Kellett et al.*, 2009]), which distinguish the detachment structures from more western Himalayan regions based on the present-day outcrop pattern where typically only one (inner) STD strand is observed. Current data regarding the timing of ductile shear on the STD in Bhutan is limited to the following areas (Figure 1): southern Lingshi klippe, southwestern Ura klippe, Masang Kang [*Kellett et al.*, 2009] and Khula Kangri [*Edwards and Harrison*, 1997]. Zircon U-Pb data from synkinematic leucogranites indicate that north vergent extensional ductile deformation associated with the outer STD lasted between at least 24 and 16 Ma, and on the inner STD between 15.5 and 11.0 Ma [*Edwards and Harrison*, 1997; *Kellett et al.*, 2009; *Kellett et al.*, 2010]. However, crystallization ages from synkinematic intrusions can only provide minimum age

[1]Department of Earth Sciences, University of St Andrews, St Andrews, UK.
[2]Department of Geology, University of Leicester, Leicester, UK.
[3]NERC Isotope Geosciences Laboratory, Nottingham, UK.
[4]Department of Earth Sciences and Environmental Sciences, Open University, Milton Keynes, UK.

0278-7407/11/2010TC002784

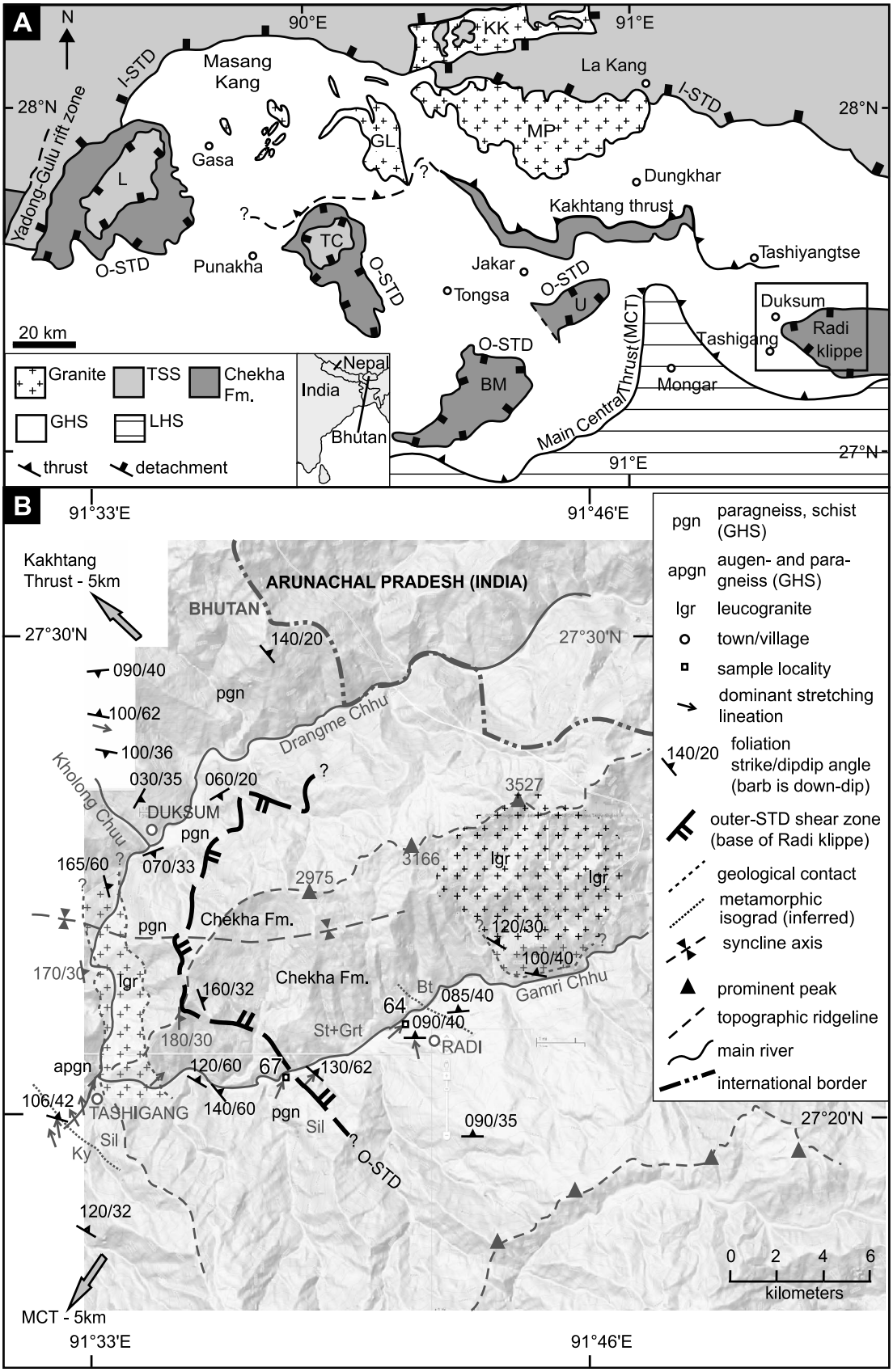
A
N
90°E
91°E
28°N
27°N
KK
La Kang
Masang Kang
I-STD
MP
GL
Gasa
L
Yadong-Gulu rift zone
Dungkhar
Kakhtang thrust
TC
Punakha
O-STD
Jakar
Tongsa
U
Tashiyangtse
Duksum
Radi klippe
Tashigang
Mongar
Main Central Thrust (MCT)
BM
20 km
Granite
TSS
Chekha Fm.
GHS
LHS
thrust
detachment
Nepal
India
Bhutan
B
91°33'E
91°46'E
27°30'N
27°20'N
Kakhtang Thrust - 5km
ARUNACHAL PRADESH (INDIA)
BHUTAN
140/20
090/40
100/62
100/36
030/35
060/20
DUKSUM
pgn
Drangme Chhu
Kholong Chuu
165/60
070/33
2975
3527
3166
lgr
120/30
100/40
Chekha Fm.
170/30
160/32
Bt
085/40
Gamri Chhu
64
090/40
RADI
St+Grt
180/30
apgn
120/60
67
130/62
106/42
TASHIGANG
140/60
Sil
Ky
090/35
120/32
MCT - 5km
paragneiss, schist (GHS)
augen- and para-gneiss (GHS)
leucogranite
town/village
sample locality
dominant stretching lineation
foliation strike/dipdip angle (barb is down-dip)
outer-STD shear zone (base of Radi klippe)
geological contact
metamorphic isograd (inferred)
syncline axis
prominent peak
topographic ridgeline
main river
international border
0 2 4 6
kilometers

Figure 1

constraints on the initiation of shearing across the STD. The minimum age of ductile deformation on the outer STD has been constrained using muscovite $^{40}Ar/^{39}Ar$ thermochronology to circa 11 Ma [*Kellett et al.*, 2009], but the true age for the cessation of ductile displacement across the outer STD may be as old as 16 Ma.

[4] Here we present U-Th-Pb in situ monazite data from metapelites located in the outer STD shear zone in the far east of Bhutan. These data, combined with geological mapping, structural geology, and detailed textural analysis constrain the initiation *and* cessation of north vergent ductile shear on the outer STD. We discuss the implications of our results for the tectonic evolution of the eastern Himalaya, while highlighting the need for precise constraints on the age and duration of displacement across shear zones in order to model orogenic processes accurately.

2. The South Tibetan Detachment

[5] The STD includes a ductile shear zone usually overprinted at higher structural levels by a discrete normal brittle fault associated with north vergent extensional movement into the upper crust [*Burchfiel et al.*, 1992]. The shear zone, although largely recognized as a north vergent extensional structure, does record an early (and/or alternating with top-to-the-northeast) top-to-the-southwest kinematic history [*Yin*, 2006; *Webb et al.*, 2007]. Amphibolite-granulite facies (generally migmatitic and mylonitic) GHS rocks lie in the footwall, juxtaposed against the Tethyan Sedimentary Series (TSS) in the hanging wall. Basal TSS rocks, where preserved between the base of the STD shear zone and the structurally higher brittle STD fault, are metamorphosed to amphibolite facies, e.g., Haimanta Group [*Chambers et al.*, 2009] and Everest Series [*Jessup et al.*, 2008]. Above the brittle STD, TSS rocks are weakly or unmetamorphosed, but do preserve multiple episodes of Eocene-Oligocene deformation in response to initial collision between India and Eurasia [e.g., *Godin*, 2003]. The age range for ductile shearing on the STD across the entire orogen is 26 to 12 Ma with most data clustering between 23 and 18 Ma [*Godin et al.*, 2006, Table 1]. The majority of these data are granite crystallization ages. Many of these granites intruded during normal shear on the STD, were deformed by ductile shearing, and crosscut by brittle STD faults. These crystallization ages therefore only represent a point in time at which the ductile STD was active, and do not provide constraints on the initiation or cessation of movement on the detachment in the midcrust; data that are key to tectonic modeling.

[6] In the eastern Himalaya, the lower (ductile) and upper (brittle) STD structures described above are recognized in the far north of Bhutan: the contact between the GHS and TSS features discrete steeply north dipping brittle faults that cut mylonitic fabrics associated with previous ductile shear along the STD shear zone [*Burchfiel et al.*, 1992; *Edwards et al.*, 1996]. Yet in more central and southern regions of Bhutan, a high-strain ductile shear zone forms the base of several isolated synformal outliers (klippen) of TSS above gneissic and migmatitic GHS (Figure 1). Following the rationale presented by *Kellett et al.* [2009], we refer to this high-strain shear zone as the outer STD, and we consider the structures in northern Bhutan to be part of the inner STD system. At the base of the klippen are garnet-staurolite schists of the Chekha Formation. Metamorphic grade and degree of deformation decrease markedly upsection into the TSS where Paleozoic fossils are preserved and sedimentary bedding is the primary planar fabric [*Hughes et al.*, 2011]. Asymmetric shear bands and deformed leucogranite veins in the klippen indicate normal displacement of the hanging wall rocks toward the north [*Grujic et al.*, 2002]. The outer STD as observed at the base of the Ura and Radi klippen lacks evidence for brittle faulting that is observed elsewhere in the Himalaya, including the inner STD in the north of Bhutan.

[7] There are two end-member models for the formation of the inner and outer strands of the STD: (1) critical taper–frictional wedge theory and (2) channel flow–viscous wedge theory, both discussed by *Kellett et al.* [2009]. In both models the outer STD is abandoned by 12 Ma, and north vergent normal shear is transferred to the inner STD, an active structure from 15.5 to 11 Ma [*Edwards and Harrison*, 1997; *Grujic et al.*, 2002; *Kellett et al.*, 2009]. In central and eastern Bhutan the termination of the outer STD is considered the result of large-scale folding of the GHS "channel" and subsequent out-of-sequence thrusting between 14 and 10 Ma, thickening the GHS along the northward dipping Kakhtang thrust, and therefore isolating klippen of TSS [*Grujic et al.*, 2002]. This hinterland propagation of exhumation and metamorphism during the Middle Miocene contrasts with the pattern of foreland-directed thrust propagation observed in more western regions of the Himalayan orogen [*Hodges*, 2000].

3. Geology of the Radi Klippe, Eastern Bhutan

[8] The Radi (or Sakteng) klippe is the easternmost klippe of TSS in Bhutan (Figure 1), and therefore probably also in the Himalayas. The basal Chekha Formation schists feature well-developed, pervasive foliation and crenulation fabrics, formed during lower amphibolite-facies metamorphism. Some garnet porphyroblasts are idioblastic, and these are restricted to quartz-rich crenulation arcs, only weakly wrapped by the matrix foliation and have no internal fabric defined by inclusions (Figure 2f). Other garnet porphyroblasts are subidioblastic and overprinted a crenulated fabric:

Figure 1. (a) Simplified geological map of Bhutan after *Bhargava* [1995] and *Hollister and Grujic* [2006]. O-STD and I-STD, outer and inner South Tibetan detachments, respectively. Geological units are as follows: TSS, Tethyan Sedimentary Series; GHS, Greater Himalayan Sequence; LHS, Lesser Himalayan Sequence. Klippen abbreviations are L, Lingshi; TC, Tang Chu; BM, Black Mountain; U, Ura. Plutons are as follows: KK, Khula Kangri; MP, Monlakarchung-Pasalum; GP, Gophu La. (b) Geology of Radi klippe (detail of boxed area in Figure 1a). Metamorphic zones labeled with mineral abbreviations according to *Kretz* [1983].

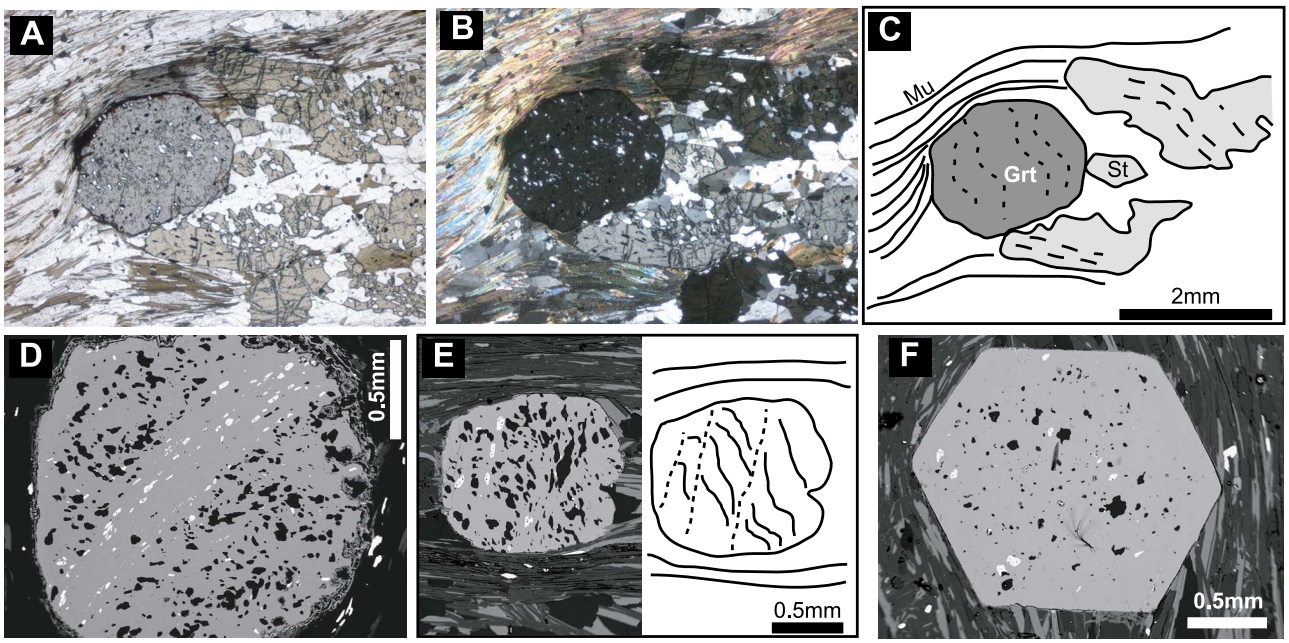

Figure 2. Microtextures in the Chekha Formation, Radi Klippe. (a) Plane-polarized microphotograph of garnet-staurolite mica schist. (b) Cross-polarized view of Figure 2a. (c) Line drawing of Figure 2a. Mineral abbreviations according to *Kretz* [1983]. Staurolite growth is posttectonic evidenced by inclusion fabric continuous with the external (matrix) fabric that is defined largely by muscovite but also biotite, plagioclase, and quartz. (d–f) Backscatter images showing garnet morphologies.

ilmenite inclusions define crenulation limbs (Figure 2e) or possible fluid pathways (Figure 2d). Poikiloblastic staurolite both encloses garnet and overprints the matrix foliation, thus postdating garnet growth and deformation (Figures 2a, 2b, and 2c). Biotite, amphibole and staurolite porphyroblasts have commonly grown across a fine-grained micaceous foliation (Figures 3b and 3c [*Gansser*, 1983]). Quartzites in the Chekha Formation are not penetratively deformed and preserve cross bedding, providing evidence for strain partitioning (Figure 3a). Further upsection (NE of Radi; Figure 1), metamorphic grade decreases into biotite-grade schists. Unmetamorphosed, potentially fossiliferous TSS, recognized in the core of other klippen (Figure 1 [*Gansser*, 1983; *Hughes et al.*, 2011]), are yet to be documented in the Radi klippe. Small (meter-scale) boudinaged leucogranite and pegmatite intrusions cut the main foliation of the Chekha Formation at an oblique angle. At least one kilometer-scale, relatively discordant, granite intrudes higher structural levels in the Chekha Formation (Figure 1b [*Bhargava*, 1995]).

[9] In contrast to the Chekha Formation schists, the footwall to the outer STD is characterized by mylonitic sillimanite gneiss of the GHS, and the shear zone can be traced based on this lithological contrast (Figures S2, S3, and S4 in Text S1).[1] The GHS rocks in the sampled area (Figure 1b) contain fibrolitic sillimanite in the matrix and matted prismatic crystals on shear surfaces (Figure S8); garnet is also abundant; no kyanite was found, although kyanite is present at structurally deeper levels in the GHS (Figure S6 [*Daniel et al.*, 2003]), and has been found in the uppermost meters of the GHS at the western boundary of the klippe [*Grujic et al.*, 2002]. Tourmaline ± white mica ± garnet leucosome pods and boudinaged veins are common. Within the GHS beneath the western edge of the Radi klippe, subparallel to the base of the klippe (Figure 1b and Figure S5 in Text S1), a ~13 Ma leucogranite occurs as a late synkinematic intrusive sheet with ~500 Ma augen gneiss xenoliths [*Daniel et al.*, 2003]. Although weakly foliated, this leucogranite appears to have intruded parallel to the strongly layered fabric of the GHS but does not intrude upward into the STD zone.

[10] In the immediate footwall to the outer STD, asymmetric foliation boudinage and shear bands in the GHS gneisses record top down to the northeast. This contrasts with lower levels in the GHS toward the MCT that consistently record south vergent thrusting (e.g., mylonitic augen gneiss with top-to-the-south sense of shear; Figure S7 in Text S1 [*Grujic et al.*, 2002]). At the base of the Chekha Formation, kinematic indicators (stretching lineations, mineral lineations and fibrous minerals) record predominantly north to northeast directed kinematics and minor conjugated south to west directed kinematics, indicating a significant pure shear component during outer STD shearing [*Grujic et al.*, 2002]. Asymmetric pressure shadows on garnet porphyroblasts in the basal Chekha Formation also record northeast vergent normal shear, but at higher structural levels in the klippe kinematic indicators are weakly developed and sense of shear is ambiguous. However,

[1]Auxiliary material data sets are available at ftp://ftp.agu.org/apend/tc/2010tc002784. Other auxiliary material files are in the HTML.

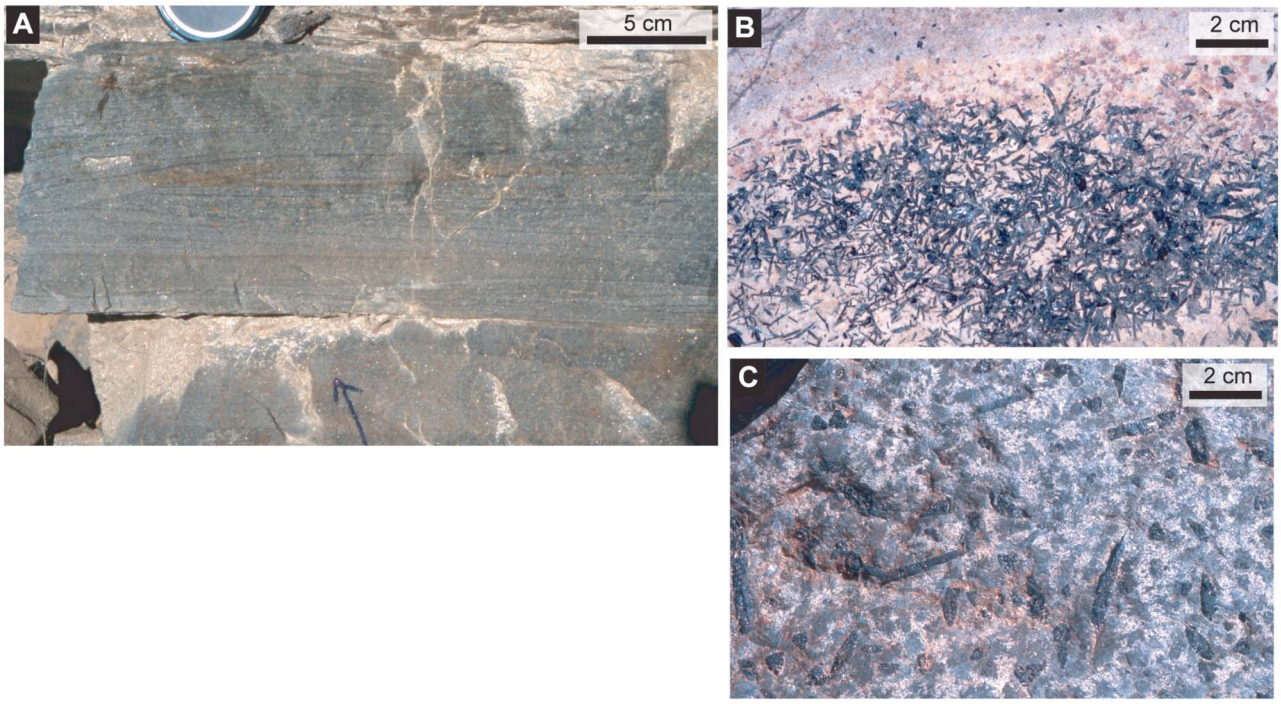

Figure 3. Photographs of the Chekha Formation, Radi Klippe. (a) Cross-bedded amphibolite-facies quartzite, several hundred meters above the base of the STD zone. (b) Randomly oriented amphibole on a surface of plagioclase-quartz-garnet metapsammite, 2 km WSW of Radi. (c) Randomly oriented staurolite crystals on a surface of biotite-plagioclase-quartz-garnet in metapelite, 2 km WSW of Radi.

asymmetric pressure shadows on garnet porphyroblasts have been observed at one locality which record top-to-the-southwest thrust kinematics.

4. Monazite Analysis

4.1. Sample Descriptions

[11] Samples of the Chekha Formation and the GHS from the outer STD shear zone, Radi klippe (Figure 1b) contain metamorphic monazite grains exclusive to the matrix; that is, they are not present as inclusions in either garnet or staurolite porphyroblasts. In the GHS (sample 67) grains are generally elongate (~50 × 100 μm), subhedral, and have weak, patchy, or no apparent Y or Th zonation (Figure 4 and Figure S1 in Text S1). In comparison, monazite grains from the Chekha Formation (sample 64) are relatively abundant, euhedral, smaller (~25 × 40–75 μm) and commonly have distinct Th zonation, corresponding in at least one grain with weak yet discernible Y zonation (Figure 4). For most monazite grains in this study Y is below the detection level. In both samples most of the grains are aligned with the matrix foliation and lineation, indicating synkinematic growth or possibly postkinematic mimetic growth (i.e., growth controlled by preexisting grain arrangements [e.g., *Passchier and Trouw*, 2005]). However, some grains in the Chekha Formation (e.g., "ChF mon1"; Figure 4) overgrew the matrix foliation and are therefore postkinematic. With regards to other accessory minerals, garnet has inclusions of allanite (both samples) and apatite (Chekha Formation only); apatite is a common matrix phase.

4.2. (U, Th)-Pb Analytical Methods

[12] A UP193SS New Wave Research laser ablation (LA) system was used in conjunction with a Nu Instruments inductively coupled plasma multicollector mass spectrometry (ICP-MC-MS) at the NERC Isotope Geosciences Laboratory, UK, to ablate single spots (15 μm diameter) in monazite grains using laser fluences of 2–3 J cm^{-2} (50% power, 5 Hz). Analysis of monazite followed methods similar to those described by *Cottle et al.* [2007] using the instrumental setup similar to *Simonetti et al.* [2005]. Inferred ages of monazite growth are based on both U-Pb and Th-Pb measurements. However, instrumental protocols meant that U-Pb and Th-Pb could not be measured simultaneously and were therefore measured sequentially, returning to the exact location to run the remaining Th-Pb analysis sequence. Only one to two analyses per sample grain were possible to ensure sputter cross contamination was avoided and in view of the small grain size of monazite.

[13] Due to the small grain sizes involved, for which it is difficult to accurately measure ^{204}Pb via LA-MC-ICP-MS, we implemented the following common ^{208}Pb correction method to determine radiogenic ^{208}Pb for ^{232}Th-^{208}Pb ages. In this procedure we (1) assumed that the lower concordia intercepts on the U-Pb Tera-Wasserburg plot represent the correct ^{238}U-^{206}Pb age of each sample, (2) calculated the

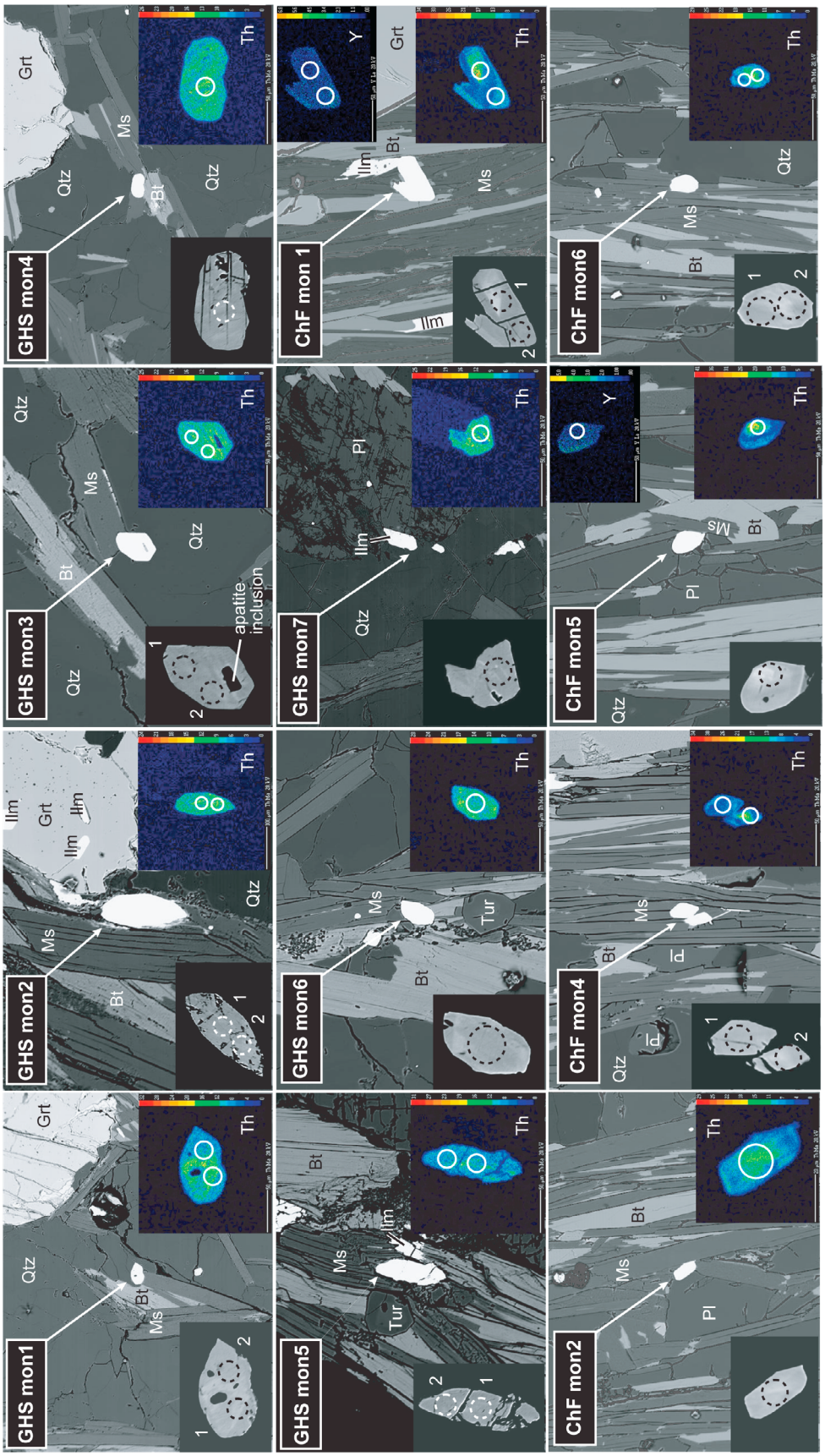

Figure 4. Backscatter electron images of monazite grains from samples 67 (GHS) and 64 (Chekha Formation). Sections were cut perpendicular to foliation and perpendicular to lineation (sample 67) or parallel to the lineation (sample 64). Left insets show enlarged high-contrast BSE images. Right insets show Th ± Y maps (brightness corresponds to concentration). Circles show locations of LA-ICPMS analyses (spot size 15 μm). See auxiliary material for more images of grains from the GHS sample 67 and color versions of the Th and Y maps. Mineral abbreviations according to *Kretz* [1983].

isotopic composition of this concordant age (i.e., free of common Pb), (3) calculated the fractional contribution of common ^{206}Pb and ^{207}Pb that contributed to the measured composition, and (4) used these common Pb contributions, and a model Pb-isotope composition for ~20 Ma [*Stacey and Kramers*, 1975], to correct the measured ^{208}Pb for common ^{208}Pb and calculate radiogenic ^{232}Th-^{208}Pb ages. As estimates of either common ^{206}Pb or common ^{207}Pb can be applied in step 3 to calculate common ^{208}Pb, two age estimates per analysis were generated.

[14] The 554 Ma Manangotry monazite standard [*Paquette et al.*, 1994; *Horstwood et al.*, 2003] and an in-house 54.5 Ma monazite standard, FC-1 were used for Pb/U and Pb/Th normalization, respectively, coupled with a static ablation pattern using identical spot size and fluence ablation characteristics. The FC-1 standard cannot be directly used for U-Pb calibration as it contains variable excess ^{206}Pb. The overall reproducibility of both standards during the course of these analyses was 2 to 8% (2σ), which has been quadratically propagated into the uncertainties for each spot analysis. These uncertainties are higher than normally observed, partly due to the very small ablation spot size used to obtain the high spatially resolved analyses. Sample data were normalized in subsessions as appropriate using the standard data over two analytical sessions.

4.3. Results

[15] Isotopic measurements for monazite samples and standards are presented in Table 1 and Data Set S1, respectively. Calculated ages and data plots were generated using Isoplot version 3.40 [*Ludwig*, 2003]. U-Pb data plotted on a Tera-Wasserburg diagram lie in two linear arrays, one corresponding to each sample: 21.6 ± 0.6 (2σ) Ma, Chekha Formation; 23.4 ± 1.2 (2σ) Ma, GHS (Figure 5). No data were omitted from the regressions on the Tera-Wasserburg plot with the exception of two analyses (5.2, 7) from the GHS sample that plot in between the two groups of data. These data are not included in the regression of data from this sample as they either represent analyses that partially sampled neighboring ilmenite (Figure 4) and were subsequently contaminated by common Pb, or analyses of uncommon grains (or younger zones of grains) that crystallized between ~23 and 22 Ma.

[16] We recognize that one analysis in the Chekha Formation sample (1.2) has high common Pb and relatively low absolute Th and U concentrations compared to the other monazite analyses (Table 1). We infer that the ablation, targeted at the grain rim (a relatively low concentration domain), partially sampled the grain boundary and adjacent mineral(s), e.g., biotite, feldspar. Whether or not we include this datum point makes no difference to the age interpretation (illustrated in Figures S9 and S10 in Text S1).

[17] The size of laser beam required to ablate an adequate amount of sample for analysis precludes isolation of the observed chemically distinct zoning (which occurs on scales of 5–10 μm), and as a result most, if not all monazite analyses represent samples of differential mixtures of these zones. However, there is no discernible pattern between these analyses, or similarly, between core and rim analyses, suggesting that zoning was acquired via growth over a very short period of time, i.e., within the errors quoted for each U-Pb age of monazite growth.

[18] Although the interpretation of ^{238}U-^{206}Pb data may be complicated by the presence of excess ^{206}Pb in Th-rich minerals such as monazite [e.g., *Parrish*, 1990], we cannot resolve any such effect in our data set. Regardless, any excess ^{206}Pb is unlikely to account for more than ~0.5 Ma difference in age, since the mean Th-Pb ages (Figure 6 and Table 2) are slightly older but agree within uncertainty, with the U-Pb ages (the opposite would be true if excess ^{206}Pb was significant). Nevertheless the quoted ages could be slightly too old (i.e., 0.5 ± 0.5 Ma).

5. Discussion

5.1. Monazite Petrogenesis

[19] Since monazite in both our samples is restricted to the matrix, and since allanite is only present as inclusions in garnet, we infer that monazite grew at the expense of matrix allanite following garnet growth [e.g., *Janots et al.*, 2008]. Combined with (1) the lack of evidence for retrograde monazite [e.g., *Bollinger and Janots*, 2006], (2) the fact that distinct Th zones within one monazite reflect discontinuous reactions during the same metamorphic event [e.g., *Foster et al.*, 2000], and (3) because rimward decrease of Th content in monazite is consistent with subsolidus crystallization during prograde metamorphism [*Kohn and Malloy*, 2004], all the analyzed monazite grains grew during prograde, near-peak metamorphism. Y zonation in garnet (Figure 7) and monazite in both samples is consistent with this reaction history, as monazite grains are depleted in Y owing to the earlier sequestration of Y in garnet.

[20] The timing of prograde monazite growth is closely associated with the staurolite-in reaction [*Corrie and Kohn*, 2008], which is consistent with the textural evidence for concurrent, late growth of both monazite and staurolite in the Chekha Formation. Th (±Y)-rich monazite rims in the Chekha Formation, indistinguishable in age from the other analyses of monazite in this sample, may be attributable to either late garnet resorption during initial decompression or the influx of Th (±Y)-rich fluids associated with local leucogranite intrusions.

[21] Assuming sufficient time since collision to allow a lateral thermal gradient to develop between the hinterland and foreland of the orogen [see *Kohn*, 2008, and references therein], regardless of the orientation of the outer STD from the horizontal, initiation of north vergent shear across the outer STD would have cooled the immediate footwall (GHS) and effectively terminated prograde monazite formation. Therefore the GHS monazite grains are prekinematic or early synkinematic with respect to north vergent STD shear. Consequently, the age of GHS monazite grains constrains the initiation of normal shear on the outer STD to between 25 and 22 Ma (Table 2). Synkinematic to postkinematic monazites from the Chekha Formation, in the immediate hanging wall to the outer STD, date cessation of normal shear on this structure at 22–20 Ma (Table 2). We attribute prograde *syn*kinematic monazite growth in the Chekha Formation to viscous heating, whereas prograde

Table 1. (U, Th)-Pb Sample Monazite Isotopic Data

										Isotopic Ratios Corrected for Mass Bias and Normalization to Standard								
Sample	^{206}Pb (mV)	^{207}Pb (mV)	^{208}Pb (mV)	^{232}Th (V)	^{238}U (mV)	Pb[a] (ppm)	Th[a] (ppm)	U[a] (ppm)	Th/U	^{207}Pb/ ^{206}Pb	1σ (%)	^{238}U/ ^{206}Pb	1σ (%)	^{207}Pb/ ^{235}U	1σ (%)	^{208}Pb/ ^{232}Th	1σ (%)	Rho
Chekha Formation (64)																		
1.1	0.42	0.13	1.1	0.50	169	187	22585	2263	10.0	0.0814	1.34	297.8	2.28	0.0337	2.65	0.00162	8.32	0.86
1.2	0.20	0.12	0.5	0.10	28	102	4317	377	11.4	0.6313	1.29	85.66	5.28	1.0162	5.44	0.00337	5.53	0.97
2	0.49	0.07	1.3	0.71	154	190	31753	2067	15.4	0.1359	5.10	267.6	2.36	0.0700	5.62	0.00122	4.91	0.42
4.1	0.39	0.07	1.0	0.53	144	189	24636	2006	12.3	0.1348	1.37	258.6	1.64	0.0719	2.14	0.00136	4.38	0.77
4.2	0.46	0.06	1.5	0.94	153	202	43954	2131	20.6	0.1419	2.11	258.7	1.63	0.0757	2.67	0.00115	1.86	0.61
5	0.47	0.05	2.3	1.39	168	215	65078	2340	27.8	0.1098	1.90	265.7	1.71	0.0570	2.55	0.00121	1.23	0.67
6.1	0.22	0.02	1.3	0.79	87	106	37261	1213	30.7	0.1007	3.45	2858	1.84	0.0486	3.91	0.00113	1.27	0.47
6.2	0.22	0.02	1.1	0.65	86	106	30570	1204	25.4	0.0963	3.62	275.9	1.83	0.0481	4.06	0.00116	1.50	0.45
GHS (67)																		
1.1	0.57	0.03	1.8	0.87	205	239	47069	2613	18.0	0.0645	2.46	268.3	1.78	0.0331	3.03	0.00114	4.39	0.59
1.2	0.53	0.04	1.5	0.66	198	235	35822	2518	14.2	0.0698	2.38	263.1	1.77	0.0366	2.97	0.00122	4.46	0.60
2.1	0.58	0.05	1.8	0.76	161	196	41233	2053	20.1	0.0693	1.77	257.2	1.79	0.0372	2.52	0.00131	4.62	0.71
2.2	0.58	0.04	1.6	0.69	225	268	37505	2858	13.1	0.0621	2.13	262.8	1.79	0.0326	2.78	0.00124	4.45	0.64
3.1	0.57	0.03	1.2	0.56	197	230	30176	2509	12.0	0.0627	2.65	261.1	2.01	0.0331	3.33	0.00122	4.33	0.61
3.2	0.45	0.03	1.4	0.68	163	72	36980	2119	17.4	0.0641	2.97	264.6	0.97	0.0334	3.12	0.00126	1.82	0.31
4	0.77	0.05	1.9	0.85	275	331	45796	3498	13.1	0.0713	1.76	257.9	1.75	0.0381	2.48	0.00124	4.41	0.71
5.1	0.63	0.04	1.3	0.64	234	67	34455	3030	11.4	0.0616	2.33	264.5	0.81	0.0321	2.47	0.00123	1.99	0.33
5.2	0.58	0.05	1.4	0.64	243	72	34632	3149	11.0	0.0914	2.05	260.3	0.90	0.0484	2.24	0.00129	1.83	0.40
6	0.62	0.04	1.9	0.82	189	93	44147	2454	18.0	0.0652	2.32	260.6	0.88	0.0345	2.48	0.00131	1.95	0.36
7	0.50	0.03	1.7	0.84	232	85	45398	3011	15.1	0.0733	2.53	288.2	0.81	0.0351	2.66	0.00116	1.97	0.31

	Uncorrected Ages (Ma)								Corrected Isotopic Ratio[b]		Corrected Age[b] (Ma)		Corrected Isotopic Ratio[c]		Corrected Age[c] (Ma)	
Sample	^{207}Pb/ ^{206}Pb	2σ abs	^{206}Pb/ ^{238}U	2σ abs	^{207}Pb/ ^{235}U	2σ abs	^{208}Pb/ ^{232}Th	2σ abs	^{208}Pb/ ^{232}Th	1σ (%)	^{208}Pb/ ^{232}Th	2σ abs	^{208}Pb/ ^{232}Th	1σ (%)	^{208}Pb/ ^{232}Th	2σ abs
Chekha Formation (64)																
1.1	1232	26	22	1.0	38	2.0	33	5.4	0.00162	8.32	32.7	5.4	0.00157	8.32	31.6	5.4
1.2	4582	19	75	7.9	712	106	68	7.5	0.00134	5.53	27.2	3.0	0.00127	5.53	25.7	3.0
2	2176	89	24	1.1	69	8.0	25	2.4	0.00112	4.91	22.6	2.2	0.00111	4.91	22.4	2.2
4.1	2162	24	25	0.8	70	3.1	27	2.4	0.00122	4.38	24.6	2.2	0.00124	4.38	25.0	2.2
4.2	2251	36	25	0.8	74	4.1	23	0.9	0.00105	1.86	21.2	0.8	0.00106	1.86	21.4	0.8
5	1796	35	24	0.8	56	2.9	24	0.6	0.00116	1.23	23.3	0.6	0.00117	1.23	23.6	0.6
6.1	1637	64	23	0.8	48	3.9	23	0.6	0.00111	1.27	22.5	0.6	0.00110	1.27	22.3	0.6
6.2	1554	68	23	0.9	48	4.0	23	0.7	0.00113	1.50	22.7	0.7	0.00113	1.50	22.8	0.7
GHS (67)																
1.1	757	104	24	0.9	33	2.0	23	2.0	0.00112	4.39	22.6	2.0	0.00112	4.39	22.7	2.0
1.2	922	98	24	0.9	36	2.2	25	2.2	0.00118	4.46	23.9	2.1	0.00120	4.46	24.2	2.1
2.1	908	73	25	0.9	37	1.9	26	2.4	0.00126	4.62	25.4	2.3	0.00128	4.62	26.0	2.3
2.2	677	91	24	0.9	33	1.8	25	2.2	0.00120	4.45	24.2	2.2	0.00122	4.45	24.6	2.2
3.1	697	113	25	1.0	33	2.2	25	2.1	0.00116	4.33	23.4	2.0	0.00119	4.33	24.0	2.0
3.2	744	126	24	0.5	33	2.1	25	0.9	0.00123	1.82	24.8	0.9	0.00124	1.82	25.0	0.9
4	965	72	25	0.9	38	1.9	25	2.2	0.00117	4.41	23.7	2.1	0.00120	4.41	24.3	2.1
5.1	659	100	24	0.4	32	1.6	25	1.0	0.00118	1.99	23.9	0.9	0.00120	1.99	24.3	0.9
5.2	1454	78	25	0.4	48	2.2	26	1.0	0.00123	1.83	24.8	0.9	0.00123	1.83	24.8	0.9
6	782	97	25	0.4	34	1.7	26	1.0	0.00126	1.95	25.5	1.0	0.00129	1.95	26.0	1.0
7	1022	103	22	0.4	35	1.9	24	0.9	0.00120	1.97	24.2	1.0	0.00114	1.97	23.1	1.0

[a]Approximately 20% uncertainty on concentration. Also note that the sample concentrations refer to material excavated during laser ablation and that the mineral concentrations may be lower than if the spot failed to be entirely within the mineral, compounded further by the consequential mismatch between sample and standard and erroneous standard normalization.
[b]Using ^{206}Pb (see text for procedural explanation).
[c]Using ^{207}Pb (see text for procedural explanation).

*post*tectonic monazite growth in the same sample is considered the product of advected heat, from the uplifted and therefore hotter GHS below, across the outer STD and into the overlying Chekha Formation. Postkinematic amphibole and staurolite in the Radi klippe (Figures 3b and 3c) are also attributed to advected heat from the GHS. Peak temperature in the Chekha Formation thus postdates peak temperature in the GHS by up to 5 Ma.

5.2. Tectonic Evolution

[22] *Kellett et al.* [2009] outline two models for the tectonic evolution of Bhutan: (1) critical taper–frictional wedge theory and (2) channel flow–viscous wedge theory. Both of these apply to a system in which the STD shear zone is a continuously active structure, since its initiation in the Late Oligocene, through transfer from the outer STD to the inner STD at 15.5 Ma, to cessation in the Middle to Late Miocene

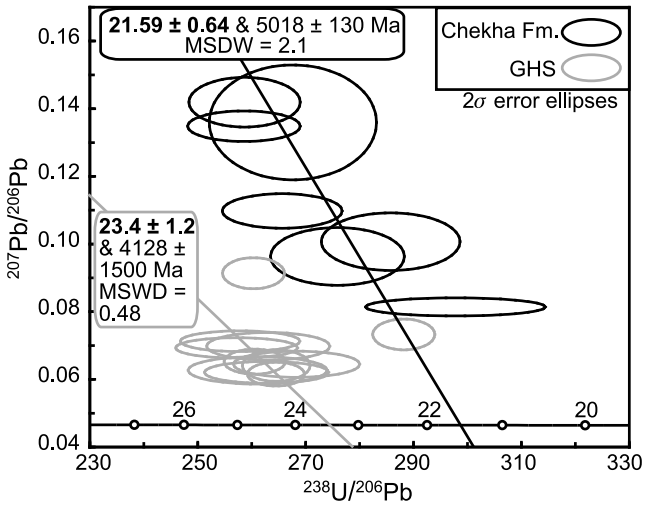

Figure 5. Tera-Wasserburg plot of U-Pb monazite data from the GHS and Chekha Formation (one analysis of which, included in the regression but with significant common Pb, is therefore not seen at this scale).

(Figure 8). Yet our data suggest that ductile normal shear across the outer STD, now preserved at the base of the Radi klippe, was pulse-like, lasting up to only 5 Ma. This part of the outer STD may represent one of several splays of the detachment, whose cumulate history was long-lasting normal shear that was localized in both space and time on different shear zones at different time intervals. Alternatively, our data highlight an apparent time gap in the eastern Bhutan Himalaya of at least 4.5 Ma before ductile normal shear on the inner STD initiated at 15.5 Ma [*Kellett et al.*, 2009]. The extent to which early (pre-16 Ma) STD shear may also be recorded within the strain history of the upper GHS beneath the inner STD, is as yet undetermined; data from *Kellett et al.* [2009] do not exclude the possibility that shear across the inner STD may have initiated earlier than 15.5 Ma and thus shared a common movement history with the outer STD. The following discussion considers the implication of a significant hiatus in north vergent normal shear for the geodynamics of the far eastern Himalaya (eastern Bhutan). Although one explanation for this hiatus could be that motion on the inner STD directly north of the Radi klippe predated that on the inner STD, 100–150 km to the west (source region of all the available data), this would imply that STD movement was diachronous (younging eastward by ~5 Ma across Bhutan) for which there is no supporting evidence.

[23] A summary of the geochronologic data from the major shear zones in the eastern Himalaya is presented in

Table 2. Summary of U-Pb and Th-Pb Monazite Ages (±2σ)

Isotope System	Chekha Formation[a]	Greater Himalayan Sequence[b]
U-Pb	21.6 ± 0.6 (MSWD = 2.1)	23.4 ± 1.2 (MSWD = 0.48)
Th-Pb[c]	circa 22 Ma	24.5 ± 0.5 (MSWD = 1.4)
Th-Pb[d]	circa 22 Ma	24.5 ± 0.7 (MSWD = 2.5)

[a]Note that Chekha Formation Th-Pb ages are approximate, as the data do not define a statistically meaningful single population (Figure 6). Sample 64.
[b]Sample 67.
[c]Corrected for common Pb using ^{206}Pb.
[d]Corrected for common Pb using ^{207}Pb.

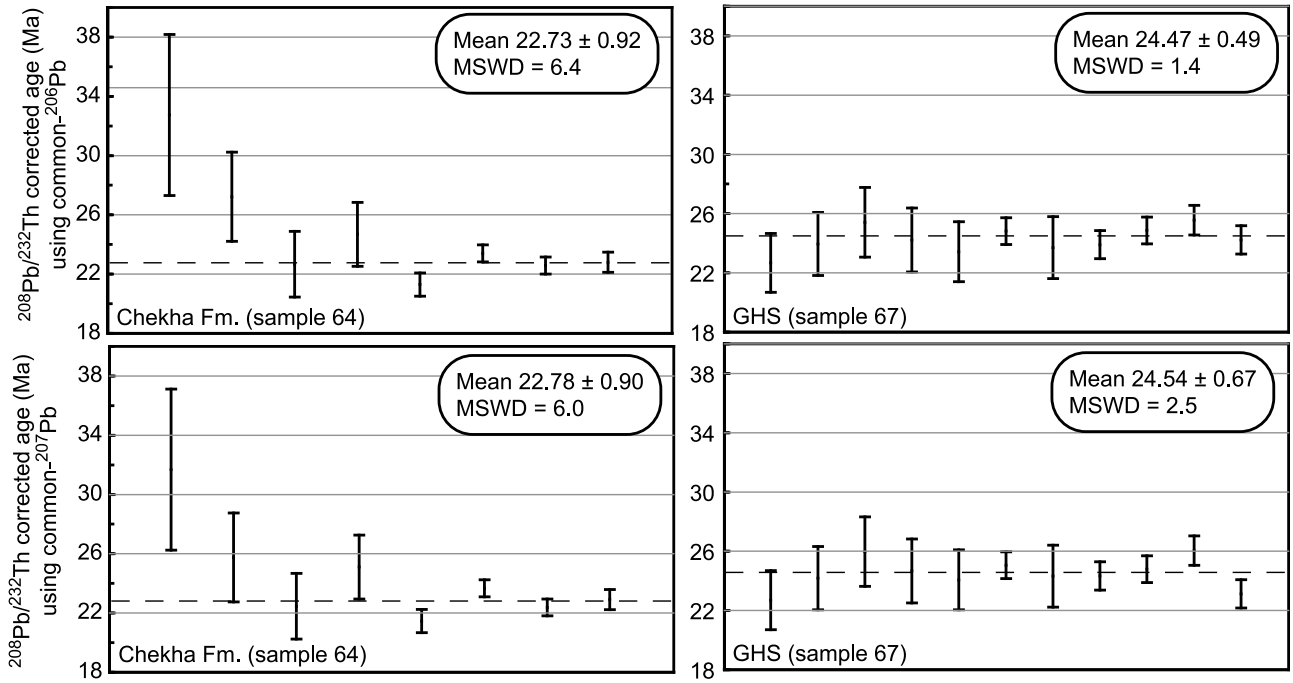

Figure 6. Weighted average ^{208}Pb/^{232}Th common Pb corrected monazite ages (Table 1). Error bars are 2σ.

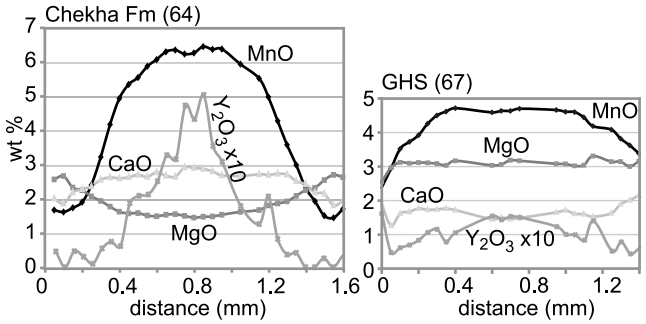

Figure 7. Major-element (Ca, Mg, and Mn) and Y profiles across garnet porphyroblasts.

Figure 8, illustrating a potentially complex interplay between the detachment faults (outer STD and inner STD) and thrust faults (MCT, KT, lower LH duplex including the Shumar thrust). It is possible that more data would reveal the longevity of the MCT-STD system throughout the Miocene, but the present data set does not unambiguously prove that this is the case. Note that we refer to *Daniel et al.* [2003] for ages relevant to shear on the MCT and KT in eastern Bhutan, and not to *Grujic et al.* [2002], who cited inaccurate age data from *Daniel et al.* [2003], which at that time was an unpublished manuscript, *in press*. Furthermore, *Daniel et al.* [2003] present no ages relevant to dating shear on the STD, and the 17–22 Ma maximum age of north vergent shearing based on a leucogranite crystallization age quoted by *Grujic et al.* [2002] is unjustified. We deliberately do not include the Main Boundary Thrust (MBT) or Main Frontal Thrust (MFT) in Figure 8, as there are no data to constrain the timing or amount of slip on these structures in the eastern Himalaya, so the geodynamics since circa 10 Ma remain difficult to interpret. Although detrital records from the western and central Himalaya suggest initiation of the MBT between 12 and 9 Ma [*Meigs et al.*, 1995; *Huyghe et al.*, 2001], kinematic reconstructions coupled with detrital records from the eastern Nepal imply that the MBT was not activated until <5 Ma [*Robinson et al.*, 2001]. Furthermore *Yin* [2006] highlights the fact that the MCT and MBT are folded in the eastern Himalaya, reflecting a major change in structural style across the orogen, and therefore age data from the western Himalaya should not be extrapolated over 1000 km to the eastern Himalaya. The one kinematic reconstruction for the eastern Himalaya by *McQuarrie et al.* [2008] implies only that shortening on the MBT and MFT occurred after 10 Ma.

[24] Across the eastern Himalaya, north vergent extension on the outer STD predates south vergent thrusting on the MCT, by at least 2 if not 6 Myr (Figure 8). Two periods of coeval shear across the outer STD and MCT can be identified between 23 and 21 Ma, and 18 and 16.5. Displacement across the MCT is also synchronous with ductile normal shear on the inner STD, between 15.5 and 14.5 Ma, and at 13.4 ± 0.2 Ma. The cessation of shearing across the MCT overlaps with initiation of the lower Lesser Himalayan duplex [*McQuarrie et al.*, 2008] for a period of 2 to 5 Ma. Initiation of south vergent thrusting on the KT occurs sometime after 15 Ma, and may have been synchronous with ductile normal shear on the inner STD. This episodic history of thrusting and extension fundamentally supports a critical taper–frictional wedge theory for the eastern Himalaya, wherein the taper of the orogenic wedge is continuously readjusted toward the critical angle through alternate, but at times coeval, thrust-detachment systems. However, during periods of coeval MCT-STD (and possibly KT inner STD) fault movement a channel flow–viscous wedge model may dominate the thermomechanic behavior of the orogenic wedge, but ultimately one of the two channel-bounding faults is deactivated; the MCT at 21 and the outer STD at ~15 Ma (Figure 8).

[25] The first transition in mode, from the critical taper–frictional wedge 1 to the channel flow–viscous wedge 1 at 23 Ma (Figure 8), may have occurred in response to the attainment of a threshold in the midcrustal to lower crustal viscosity in the Himalayan hinterland, such that ductile flow toward the topographic front between coeval structures (the MCT and STD) became the dominant exhumation mechanism (conceptually representing the denudation-driven "channel flow model" [*Beaumont et al.*, 2001]). Yet from 21 to 18 Ma there is no evidence to suggest the MCT was

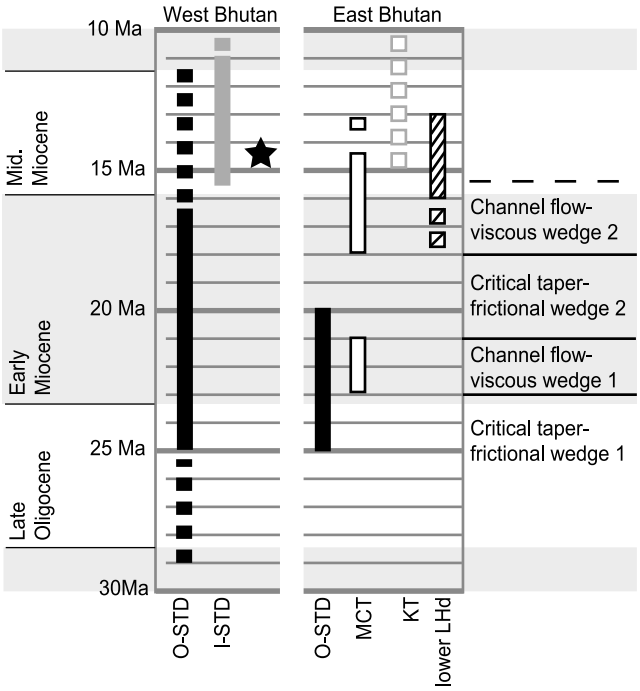

Figure 8. Timeline of movement on major structures in the eastern Himalaya, divided into west [*Edwards and Harrison*, 1997; *Kellett et al.*, 2009] and east Bhutan [*Stüwe and Foster*, 2001; *Daniel et al.*, 2003; *McQuarrie et al.*, 2008] (also this study). Bars show known bracketed ages; dashed bars show poorly constrained ages (e.g., only minimum or maximum ages of displacement known). O-STD and I-STD, outer and inner South Tibetan detachments, respectively. MCT, Main Central Thrust; KT, Kakhtang Thrust; lower LHd, lower Lesser Himalayan duplex. Black star represents timing of high-pressure metamorphism (eclogite facies) for GHS now exposed in NW Bhutan [*Grujic et al.*, 2010].

active, which effectively "turned off" channel flow toward the topographic front, and the system returned to one dominated by a critical taper–frictional wedge (#2, Figure 8). A change in one or more boundary conditions (such as focal area of denudation, denudation rate, rheology of the deforming crust) at this time would permit such an adjustment of the orogenic wedge.

[26] At 18 Ma the channel flow mode was "turned on" again (channel flow–viscous wedge 2; Figure 8). At this time the lower Lesser Himalayan duplex began to grow [*McQuarrie et al.*, 2008] leading to the formation of a ramp on the MCT. Consequently, the ductile GHS in the MCT hanging wall was destabilized and the GHS channel domed, leading to the termination of motion on the outer STD and initiation of the inner STD [*Kellett et al.*, 2009]. Thus, this channel flow–viscous wedge 2 lasted between 2 and 5 Ma, before the geodynamics changed again at ~15 Ma, either to another critical taper–frictional wedge, or a channel flow–viscous wedge bounded by the inner STD and Kakhtang Thrust. This change coincides with the exhumation of high-pressure GHS rocks at 14–15 Ma, now exposed in the NW of Bhutan [*Grujic et al.*, 2010].

[27] It is apparent that data from elsewhere in the Himalaya, which constrain both initiation *and* cessation of movement on major structures, are now required for a more detailed comparison between regions of the Himalayan orogen. However, we do not know if the outer STD and klippen of the TSS ever existed in the central or western Himalaya. The TSS klippen (including the Chekha Formation) in the eastern Himalaya may be only locally preserved due to relatively low erosion rates in this region, influenced by the uplift of the Shillong Plateau and an associated decrease in precipitation at circa 5 Ma [*Grujic et al.*, 2006; *Biswas et al.*, 2007], despite relatively high modern-day annual precipitation rates, at least in southern Bhutan, compared to central and western Himalayan regions [*Bookhagen*, 2010].

6. Conclusions

[28] Monazite U-Th-Pb data, from the outer STD at the base of the Radi klippe in the eastern Himalaya, bracket the initiation (25–22 Ma) and cessation (22–20 Ma) of north vergent normal displacement across the shear zone. South vergent thrusting on the MCT during this time supports a channel flow–viscous wedge model, but extrusion by this mechanism was apparently not sustained. Following examination of all available geochronologic data from the eastern Himalayan, we suggest that the tectonics in this region alternated between one dominated by critical taper–frictional wedge tectonics and one dominated by channel flow–viscous wedge tectonics, over time spans of circa 2–5 Ma, from the Late Oligocene to the Late Miocene. Although Early Miocene tectonics are comparable across the Himalayan orogen, a fundamental change in the pattern of exhumation occurred in the Middle Miocene between the eastern Himalaya and more western regions in the orogen that is yet to be fully understood and incorporated into geodynamic models for orogenesis.

[29] **Acknowledgments.** Field work was supported by a NERC Research Studentship field grant (J.C.) and a NERC research grant NE/C513942/1 (T.A. and N.H.). Analytical work at NIGL in the UK was supported by NIGF grant IP/868/1105 and underpinned by facility funding from NERC. The authors thank Dorji Wangda, Director of the Bhutan Department of Geology and Mines for generous permission to allow export of samples and for the privilege of engaging in field work. We are also grateful to two anonymous reviews and editorial comments resulting in an improved manuscript.

References

Beaumont, C., R. A. Jamieson, M. H. Nguyen, and B. Lee (2001), Himalayan tectonics explained by extrusion of a low-viscosity crustal channel coupled to focused surface denudation, *Nature*, *414*(6865), 738–742, doi:10.1038/414738a.

Bhargava, O. N. (Ed.) (1995), *The Bhutan Himalaya: A Geological Account*, 245 pp., Geol. Surv. of India, Calcutta, India.

Biswas, S., I. Coutand, D. Grujic, C. Hager, D. Stöckli, and B. Grasemann (2007), Exhumation and uplift of the Shillong plateau and its influence on the eastern Himalayas: New constraints from apatite and zircon (U-Th-[Sm])/He and apatite fission track analyses, *Tectonics*, *26*, TC6013, doi:10.1029/2007TC002125.

Bollinger, L., and E. Janots (2006), Evidence for Mio-Pliocene retrograde monazite in the Lesser Himalaya, far western Nepal, *Eur. J. Mineral.*, *18*, 289–297, doi:10.1127/0935-1221/2006/0018-0289.

Bookhagen, B. (2010), Appearance of extreme monsoonal rainfall events and their impact on erosion in the Himalaya, *Geomatics Nat. Hazards Risk*, *1*, 37–50, doi:10.1080/19475701003625737.

Burchfiel, B. C., B. Chen, K. V. Hodges, L. Yuping, L. H. Royden, D. Changrong, and X. Jiene (1992), The South Tibetan detachment system, Himalayan orogen: Extension contemporaneous with and parallel to shortening in a collisional mountain belt, *Spec. Pap. Geol. Soc. Am.*, *269*, 1–41.

Chambers, J. A., M. Caddick, T. Argles, M. Horstwood, S. Sherlock, N. Harris, R. Parrish, and T. Ahmad (2009), Empirical constraints on extrusion mechanisms from the upper margin of an exhumed high-grade orogenic core, Sutlej Valley, NW India, *Tectonophysics*, *477*, 77–92, doi:10.1016/j.tecto.2008.10.013.

Corrie, S. L., and M. J. Kohn (2008), Trace-element distributions in silicates during prograde metamorphic reactions: Implications for monazite formation, *J. Metamorph. Geol.*, *26*(4), 451–464, doi:10.1111/j.1525-1314.2008.00769.x.

Cottle, J. M., M. P. Searle, M. S. Horstwood, D. J. Waters, S. R. Noble, and R. R. Parrish (2007), U(-Th)-Pb age constraints on the timing and duration of channel flow in the Mt. Everest region, eastern Himalaya, *Eos Trans. AGU*, *88*(52), Fall Meet. Suppl., Abstract T34C-06.

Daniel, C. G., L. S. Hollister, R. R. Parrish, and D. Grujic (2003), Exhumation of the Main Central Thrust from lower crustal depths, eastern Bhutan Himalaya, *J. Metamorph. Geol.*, *21*(4), 317–334, doi:10.1046/j.1525-1314.2003.00445.x.

Edwards, M. A., and T. M. Harrison (1997), When did the roof collapse? Late Miocene north-south extension in the high Himalaya revealed by Th-Pb monazite dating of the Khula Kangri granite, *Geology*, *25*(6), 543–546, doi:10.1130/0091-7613(1997)025<0543:WDTRCL>2.3.CO;2.

Edwards, M. A., W. S. F. Kidd, J. Li, Y. Yu, and M. Clark (1996), Multi-stage development of the southern Tibet detachment system near Khula Kangri: New data from Gonto La, *Tectonophysics*, *260*, 1–19, doi:10.1016/0040-1951(96)00073-X.

Foster, G., P. Kinny, D. Vance, C. Prince, and N. Harris (2000), The significance of monazite U-Th-Pb age data in metamorphic assemblages: A combined study of monazite and garnet chronometry, *Earth Planet. Sci. Lett.*, *181*(3), 327–340, doi:10.1016/S0012-821X(00)00212-0.

Gansser, A. (1983), *Geology of the Bhutan Himalaya*, 180 pp., Birkhauser, Boston, Mass.

Godin, L. (2003), Structural evolution of the Tethyan sedimentary sequence in the Annapurna area, central Nepal Himalaya, *J. Asian Earth Sci.*, *22*(4), 307–328, doi:10.1016/S1367-9120(03)00066-X.

Godin, L., D. Grujic, R. D. Law, and M. P. Searle (2006), Channel flow, extrusion, and exhumation in continental collision zones: An introduction, in *Channel Flow, Ductile Extrusion and Exhumation in Continental Collision Zones*, edited by R. D. Law, M. P. Searle, and L. Godin, *Geol. Soc. Spec. Publ.*, *268*, 1–23.

Grujic, D., L. S. Hollister, and R. R. Parrish (2002), Himalayan metamorphic sequence as an orogenic channel: Insight from Bhutan, *Earth Planet. Sci. Lett.*, *198*(1–2), 177–191, doi:10.1016/S0012-821X(02)00482-X.

Grujic, D., I. Coutand, B. Bookhagen, S. Bonnet, A. Blythe, and C. Duncan (2006), Climatic forcing of erosion, landscape, and tectonics in the Bhutan

Himalayas, *Geology*, *34*(10), 801–804, doi:10.1130/G22648.1.

Grujic, D., C. Warren, and J. L. Wooden (2010), Dating the depths of the Himalayan orogen, *Geochim. Cosmochim. Acta*, *74*(11), suppl. 1, A472.

Heim, A., and A. Gansser (1939), *Central Himalaya: Geological Observations of the Swiss Expedition, 1936*, *Mem. Soc. Helvétique Sci. Nat.*, vol. 73, 245 pp., Hindustan, Delhi, India.

Hodges, K. V. (2000), Tectonics of the Himalaya and southern Tibet from two perspectives, *Geol. Soc. Am. Bull.*, *112*, 324–350, doi:10.1130/0016-7606(2000)112<324:TOTHAS>2.0.CO;2.

Hollister, L. S., and D. Grujic (2006), Pulsed channel flow in Bhutan, in *Channel Flow, Ductile Extrusion and Exhumation in Continental Collision Zones*, edited by R. D. Law, M. P. Searle, and L. Godin, *Geol. Soc. Spec. Publ.*, *268*, 415–423.

Horstwood, M. S. A., G. L. Foster, R. R. Parrish, S. R. Noble, and G. M. Nowell (2003), Common-Pb corrected in situ U-Pb accessory mineral geochronology by LA-MC-ICP-MS, *J. Anal. At. Spectrom.*, *18*(8), 837–846, doi:10.1039/b304365g.

Hughes, N. C., P. M. Myron, N. R. Mckenzie, D. A. T. Harper, O. N. Bhargava, S. K. Tangri, K. S. Ghalley, and C. M. Fanning (2011), Cambrian rocks and faunas of the Wachi La, Black Mountains, Bhutan, *Geol. Mag.*, doi:10.1017/S0016756810000750, in press.

Huyghe, P., A. Galy, J. L. Mugnier, and C. France-Lanord (2001), Propagation of the thrust system and erosion in the Lesser Himalaya: Geochemical and sedimentological evidence, *Geology*, *29*(11), 1007–1010, doi:10.1130/0091-7613(2001)029<1007:POTTSA>2.0.CO;2.

Jamieson, R. A., C. Beaumont, S. Medvedev, and M. H. Nguyen (2004), Crustal channel flows: 2. Numerical models with implications for metamorphism in the Himalayan-Tibetan orogen, *J. Geophys. Res.*, *109*, B06407, doi:10.1029/2003JB002811.

Janots, E., M. Engi, A. Berger, J. Allaz, J.-O. Schwarz, and C. Spandler (2008), Prograde metamorphic sequence of REE minerals in pelitic rocks of the Central Alps: Implications for allanite-monazite-xenotime phase relations from 250 to 610°C, *J. Metamorph. Geol.*, *26*(5), 509–526, doi:10.1111/j.1525-1314.2008.00774.x.

Jessup, M. J., J. M. Cottle, M. P. Searle, R. D. Law, D. L. Newell, R. J. Tracy, and D. J. Waters (2008), P-T-t-D paths of the Everest series schist, Nepal, *J. Metamorph. Geol.*, *26*(7), 717–739, doi:10.1111/j.1525-1314.2008.00784.x.

Kellett, D., D. Grujic, and S. Erdmann (2009), Miocene structural reorganization of the South Tibetan detachment, eastern Himalaya: Implications for continental collision, *Lithosphere*, *1*(5), 259–281, doi:10.1130/L56.1.

Kellett, D. A., D. Grujic, C. Warren, J. Cottle, R. Jamieson, and T. Tenzin (2010), Metamorphic history of a syn-convergent orogen-parallel detachment: The South Tibetan detachment system, Bhutan Himalaya, *J. Metamorph. Geol.*, *28*(8), 785–808, doi:10.1111/j.1525-1314.2010.00893.x.

Kohn, M. J. (2008), P-T-t data from central Nepal support critical taper and repudiate large-scale channel flow of the Greater Himalayan sequence, *Geol. Soc. Am. Bull.*, *120*, 259–273, doi:10.1130/B26252.1.

Kohn, M. J., and M. A. Malloy (2004), Formation of monazite via prograde metamorphic reactions among common silicates: Implications for age determinations, *Geochim. Cosmochim. Acta*, *68*(1), 101–113, doi:10.1016/S0016-7037(03)00258-8.

Kretz, R. (1983), Symbols for rock-forming minerals, *Am. Mineral.*, *68*(1–2), 277–279.

Leloup, P. H., G. Mahéo, N. Arnaud, E. Kali, E. Boutonnet, D. Liu, X. Liu, and H. Li (2010), The South Tibet detachment shear zone in the Dinggye area: Time constraints on extrusion models of the Himalayas, *Earth Planet. Sci. Lett.*, *292*(1–2), 1–16.

Ludwig, K. R. (2003), *Users Manual for Isoplot/Ex Version 3.0: A Geochronological Toolkit for Microsoft Excel*, 70 pp., Berkeley Geochronol. Cent., Berkeley, Calif.

McQuarrie, N., D. Robinson, S. Long, T. Tobgay, D. Grujic, G. Gehrels, and M. Ducea (2008), Preliminary stratigraphic and structural architecture of Bhutan: Implications for the along strike architecture of the Himalayan system, *Earth Planet. Sci. Lett.*, *272*(1–2), 105–117, doi:10.1016/j.epsl.2008.04.030.

Meigs, A. J., D. W. Burbank, and R. A. Beck (1995), Middle-late Miocene (>10 Ma) formation of the Main Boundary Thrust in the western Himalaya, *Geology*, *23*(5), 423–426, doi:10.1130/0091-7613(1995)023<0423:MLMMFO>2.3.CO;2.

Najman, Y., et al. (2010), Timing of India-Asia collision: Geological, biostratigraphic, and palaeomagnetic constraints, *J. Geophys. Res.*, *115*, B12416, doi:10.1029/2010JB007673.

Paquette, J. L., A. Nedelec, B. Moine, and M. Rakotondrazafy (1994), U-Pb, single zircon Pb-evaporation, and Sm-Nd isotopic study of a granulite domain in SE Madagascar, *J. Geol.*, *102*(5), 523–538, doi:10.1086/629696.

Parrish, R. R. (1990), U-Pb dating of monazite and its application to geological problems, *Can. J. Earth Sci.*, *27*, 1431–1450.

Passchier, C. W., and R. A. J. Trouw (2005), *Microtectonics*, 2nd ed., Springer, Berlin.

Robinson, D. M., P. G. DeCelles, P. J. Patchett, and C. N. Garzione (2001), The kinematic evolution of the Nepalese Himalaya interpreted from Nd isotopes, *Earth Planet. Sci. Lett.*, *192*(4), 507–521, doi:10.1016/S0012-821X(01)00451-4.

Simonetti, A., L. M. Heaman, R. P. Hartlaub, R. A. Creaser, T. G. MacHattie, and C. Bohm (2005), U-Pb zircon dating by laser ablation-MC-ICP-MS using a new multiple ion counting Faraday collector array, *J. Anal. At. Spectrom.*, *20*(8), 677–686, doi:10.1039/b504465k.

Stacey, J. S., and J. D. Kramers (1975), Approximation of terrestrial lead isotope evolution by a two-stage model, *Earth Planet. Sci. Lett.*, *26*(2), 207–221, doi:10.1016/0012-821X(75)90088-6.

Stüwe, K., and D. Foster (2001), $^{40}Ar/^{39}Ar$, pressure, temperature and fission track constraints on the age and nature of metamorphism around the Main Central Thrust in the eastern Bhutan Himalaya, *J. Asian Earth Sci.*, *19*(1–2), 85–95, doi:10.1016/S1367-9120(00)00018-3.

Webb, A. G., A. Yin, T. M. Harrison, J. Celerier, and P. W. Burgess (2007), The leading edge of the Greater Himalayan crystalline complex revealed in the NW Indian Himalaya: Implications for the evolution of the Himalayan orogen, *Geology*, *35*(10), 955–958, doi:10.1130/G23931A.1.

Yin, A. (2006), Cenozoic tectonic evolution of the Himalayan orogen as constrained by along-strike variation of structural geometry, exhumation history, and foreland sedimentation, *Earth Sci. Rev.*, *76*(1–2), 1–131, doi:10.1016/j.earscirev.2005.05.004.

T. Argles and N. Harris, Department of Earth Sciences and Environmental Sciences, Open University, Milton Keynes MK7 6AA, UK.

J. Chambers, Department of Earth Sciences, University of St Andrews, St Andrews KY16 9AL, UK. (jennifer.chambers@st-andrews.ac.uk)

M. Horstwood and R. Parrish, NERC Isotope Geosciences Laboratory, Keyworth, Nottingham NG12 5GG, UK.